Sensors and Actuators B 181 (2013) 802–809

Contents lists available at SciVerse ScienceDirect

Sensors and Actuators B: Chemical

journal homepage: www.elsevier.com/locate/snb

Highly sensitive humidity sensor based on high surface area mesoporous $LaFeO_3$ prepared by a nanocasting route

Jing Zhao[a], Yinping Liu[a], Xiaowei Li[a], Geyu Lu[a,*], Lu You[a], Xishuang Liang[a], Fengmin Liu[a], Tong Zhang[a], Yu Du[b,*]

[a] State Key Laboratory on Integrated Optoelectronics, College of Electronic Science and Engineering, Jilin University, 2699 Qianjin Street, Changchun 130012, China
[b] Department of Applied Physics, Shenzhen University, Shenzhen 518060, China

ARTICLE INFO

Article history:
Received 5 July 2012
Received in revised form 23 January 2013
Accepted 19 February 2013
Available online 28 February 2013

Keywords:
Mesoporous
$LaFeO_3$
High surface area
Humidity sensor

ABSTRACT

Mesoporous $LaFeO_3$ with high surface area and pore volume was prepared through a nanocasting route by using mesoporous silica SBA-15 as a hard template. The structure and chemical composition of the sample were characterized by X-ray diffraction (XRD), nitrogen adsorption–desorption, transmission electron microscopy (TEM) and inductively coupled plasma mass spectrometry (ICP-MS). The humidity sensing properties of the mesoporous $LaFeO_3$ were investigated. Impedance greatly changes by more than five orders magnitude (1.7×10^6 to 4.5 kΩ) when the relative humidity varies from 11% to 98% at 10 Hz, and it also exhibits the satisfactory response time, hysteresis and stability. The sensor utilizing mesoporous $LaFeO_3$ via nanocasting method displays superior humidity performance compared to that using bulk $LaFeO_3$ via sol–gel technique. Such sensing behavior of the mesoporous $LaFeO_3$ can be attributed to the high surface area (83.2 m^2/g) and porosity, which lead to highly effective interaction between the water molecules and the surface active sites. A possible mechanism is discussed to explain the excellent performance of the humidity sensing device using the mesoporous $LaFeO_3$.

1. Introduction

Humidity sensors play a vital role in numerous fields [1,2] to maintain a specific conditions, such as environmental monitoring, food processing industries, medicine, meteorology and research labs. The relative humidity (RH) [3], which is the ratio of actual water vapor pressure to the saturated vapor pressure at a given temperature, is the most important parameter in specifying humidity. Many types of humidity sensing devices, including ceramic [4–6], polymer [7], optical type sensors [8,9] and mechanical hygrometer [10] have been exploited to detect humidity in the practical environment. Among the various humidity sensors, the ceramic sensors are widely applied because of their simple structure, low cost and good stability. However, further investigation is requested in order to optimize the performance of ceramic humidity sensors, such as sensitivity, reversibility, long-term stability as well as response and recovery times [11]. The change of the electrical signal (impedance) with humidity in the ceramic humidity sensors is originated by the adsorption of water molecules existing in the atmosphere on the surface of the sensing materials [12,13]. Therefore, an increased specific surface area [14] and the porous structure [15] of the sample are beneficial to the sensing properties of the humidity sensor owing to the exposure of more active sites to the adsorbed water molecules.

Mesoporous materials [16,17] have received enormous attention due to their high internal and external surface area, large pore volume, uniform pore diameter and easy surface functionalization, rendering the unique materials useful in wide spectrum of fields. Recently, various mesoporous metal oxides have been largely replicated via nanocasting method [18,19] which is an important strategy for synthesizing nonsiliceous mesoporous oxides. In this route, mesoporous silicas (SBA-15, KIT-6 and MCM-41) or carbons (CMK-3) are usually used as the "hard templates" [20–24]. The precursor compound (metal salt) for the desired metal oxide is introduced into the void mesoporous channel of silica or carbon templates, and subsequent in situ thermal processing to form the desired crystalline metal oxide. Mesoporous silica template is removed using an aqueous NaOH or HF solution and carbon template is removed by calcination. A negative ordered array of the metal oxide is obtained by replicating the ordered mesostructure of the hard template. In the conventional sol–gel processes by using surfactants and block copolymers ("soft templates"), it is difficult to obtain crystalline walls or ordered mesostructure for many non-siliceous mesoporous metal oxides [25,26]. The main problem is that temperatures required for the crystallization of metal oxides are normally high and the liquid crystal surfactant templates would decompose before the crystallization of metal oxides. However, when mesoporous silicas are used as the hard

* Corresponding authors. Tel.: +86 431 85167808; fax: +86 431 85167808.
E-mail addresses: lugy@jlu.edu.cn (G. Lu), duyu@szu.edu.cn (Y. Du).

0925-4005/$ – see front matter © 2013 Elsevier B.V. All rights reserved.
http://dx.doi.org/10.1016/j.snb.2013.02.077

templates, crystals of metal oxides can grow inside the pores of the silica templates and the walls of the template can support the structure of metal oxides in the crystallization process even at high temperatures. Therefore, the hard template method is suitable for producing crystalline mesoporous metal oxides. Some typical mesoporous metal oxides with interesting functionalities, such as SnO_2 [27], In_2O_3 [28], WO_3 [29] and $LaCoO_3$ [30] have been synthesized via nanocasting method, which indicate some significant potential applications in many fields.

Perovskite-type oxides [31–34] (ABO_3, A – rare earth, alkali and alkaline earth and B – transition metal) exhibit high catalytic activity, thermal stability and low cost, which inspire many explorations of their broad utilities, such as sensors, catalysts, ferroelectric material and fuel cells. As typical perovskite oxides, $LaFeO_3$ and the related compounds [35–38] have been frequently used as chemical sensors for detection of humidity, alcohol and gases, including CO, CH_4 and NO_2. However, perovskites prepared by conventional synthetic methods still have low specific surface areas, generally below 10 m^2/g [39], which limit their efficiency in potential applications. In recent years, different synthetic routes [30,40] have been developed to increase the specific surface areas of the perovskites. Taking into account the above considerations, an effective strategy is to synthesize the porous materials in order to obtain the higher specific surface areas.

In this paper, the mesoporous $LaFeO_3$ with high surface areas, high pore volume and crystalline walls was successfully prepared through nanocasting method by using mesoporous SBA-15 as a hard template. The humidity sensing properties and mechanism of the mesoporous $LaFeO_3$ are also investigated. As a result, the sensor utilizing mesoporous $LaFeO_3$ exhibits excellent humidity activity in contrast to that based on the bulk $LaFeO_3$ synthesized using conventional sol–gel method.

2. Experimental

2.1. Preparation of materials

The hexagonal mesoporous SBA-15 silica as hard template was prepared in a modification according to the previously report [41]. In a typical synthesis process, 2 g of Pluronic P123 ($EO_{20}PO_{70}EO_{20}$, MW = 5800, Sigma–Aldrich) was dissolved in 60 mL of HCl (2 M) under stirring at 40 °C for 2 h. After addition of 4.25 g tetraethyl orthosilicate (TEOS) into the above solution, the mixture was stirring at 40 °C for another 24 h. The resulted gel was transferred into a closed Teflon-lined stainless steel autoclave and subsequently heated at 100 °C for 24 h under a static condition. Finally, the solid product was filtered off, washed with deionized water, dried, and sintered at 650 °C for 6 h.

The mesoporous $LaFeO_3$ was synthesized via nanocasting method. Typically, lanthanum nitrate, ferric nitrate and citric acid were dissolved in a mixture of ethanol and deionized water to form a homogeneous solution, and the molar ratio of citric acid to metal ions was 1:1. After stirring for 2 h, 0.5 g of SBA-15 was added to the above solution and continuously stirring at 40 °C until all the solvent was evaporated, dried at 80 °C, and calcined at 500 °C for 3 h. To achieve higher loadings, the filling procedure was repeated following the same conditions but the amount of precursor was reduced by half. Sequentially, the resultant powder was calcined at 700 °C for 3 h. Finally, the silica template was removed using excess NaOH solution (2 M). The conventional bulk $LaFeO_3$ was prepared by the sol–gel method [42] and calcined at the same temperature.

2.2. Characterization

X-ray diffraction (XRD) patterns were recorded on a Rigaku D/MAX-2550 diffractometer using Cu Kα radiation ($\lambda = 0.15418$ nm). Nitrogen adsorption–desorption isotherms were measured using a Micromeritics Gemini VII surface area and porosity system by high purity nitrogen as adsorbate at 77 K. The specific surface area was estimated by the five point Brunauer–Emmett–Teller (BET) method, and the pore size distribution was derived from the desorption branch of the isotherms by using the Barrett–Joyner–Halenda (BJH) analysis. Transmission electron microscopy (TEM) images were performed on a JEOL TEM-3010 instrument, operating at an acceleration voltage of 200 kV. Element analysis was carried out on a PerkinElmer Optima 3300 DV Inductively coupled plasma mass spectrometry (ICP-MS) instrument.

Table 1
The textural properties of the samples.

Sample	Surface area (m^2/g)	Pore size (nm)	Pore volume (cm^3/g)
SBA-15	651	6.7	0.9
Mesoporous $LaFeO_3$	83.2	4.9	0.22
Bulk $LaFeO_3$	7.8	–	0.04

2.3. Fabrication and measurement of humidity sensors

The as-synthesized samples were mixed with ethanol to form paste, and then the paste was coated onto the substrate (10 mm × 5 mm × 0.5 mm) with two Ag–Pd interdigital electrodes. Before the sensing test, all the humidity sensors were aged with a voltage AC 1 V for 24 h under 98% RH vapor environment. The characteristic curves of humidity response were carried out by a Solartron SI 1287 electrochemical interface and a Solartron SI 1260 impedance/gain-phase analyzer using Zplot software. The operation voltage was AC 1 V and the operation frequency was alterable. All the humidity sensitivity measurements were performed at room temperature. The sensor response was defined as the ratio of the impedance in 11% RH to that in the 98% RH. The controlled humidity environment was achieved by supersaturated aqueous solutions of LiCl, $MgCl_2$, NaBr, NaCl, KCl and K_2SO_4 in a closed glass vessel at room temperature (20 °C), which yielded approximately 11%, 33%, 59%, 75%, 85% and 98% relative humidity, respectively.

3. Results and discussion

3.1. Structure and morphology of as-prepared materials

Fig. 1a shows the small-angle XRD patterns of SBA-15 and mesoporous $LaFeO_3$. One diffraction reflexes of mesoporous $LaFeO_3$ is observed which can be indexed as the (1 0 0) reflection, and the (1 1 0), (2 0 0) diffraction reflexes have diminished compare to the template SBA-15. It means that the mesoporous $LaFeO_3$ has been successfully replicated from SBA-15 template and the ordering of the pore array is decreased. The wide-angle XRD patterns of mesoporous $LaFeO_3$ in Fig. 1b exhibits the diffraction pattern of crystalline perovskite-type $LaFeO_3$ (JCPDS No. 37-1493), indicating that the lanthanum and ferric precursor has been completely transformed into crystalline $LaFeO_3$ and no other crystalline phases are formed.

The nitrogen adsorption–desorption isotherms and the corresponding pore size distribution of the SBA-15 and mesoporous $LaFeO_3$ are shown in Fig. 2. The sorption isotherms of all the samples present the typical type IV shape with H1 hysteresis loops, which is the characteristic of mesoporous structure. The BET surface area, pore volume and pore size distribution of the template SBA-15, mesoporous $LaFeO_3$ and bulk $LaFeO_3$ are list in Table 1. The mesoporous $LaFeO_3$ has a relatively lower specific surface area and total pore volume than SBA-15, mainly due to the fact that the

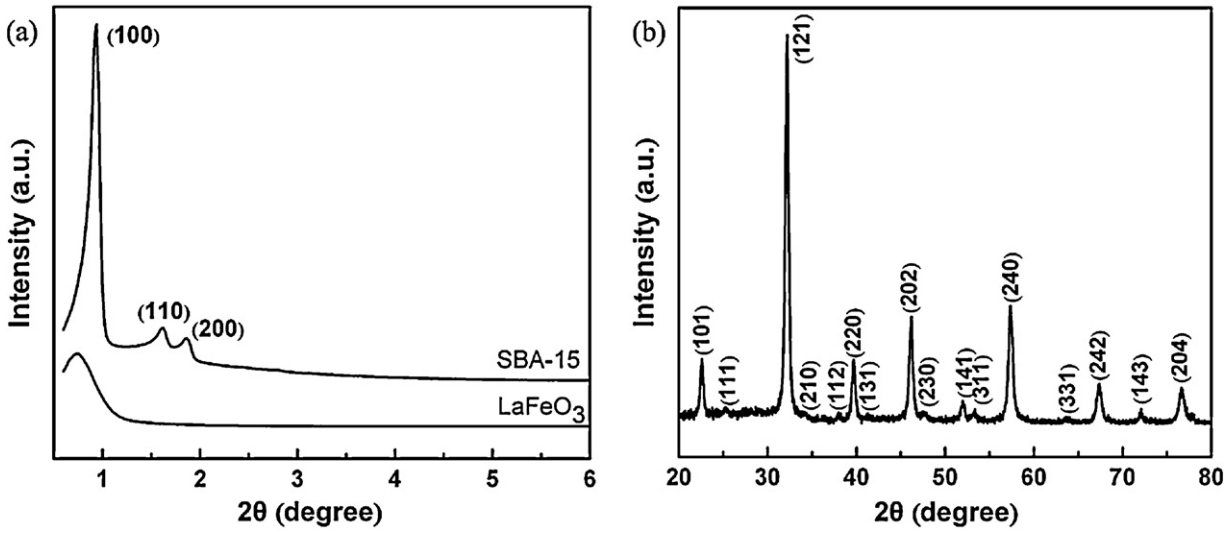

Fig. 1. (a) Small-angle XRD patterns of SBA-15 and mesoporous $LaFeO_3$ and (b) Wide-angle XRD patterns of mesoporous $LaFeO_3$.

density of bulk $LaFeO_3$ is higher than that of bulk silica (6.64 and 2.26 g/cm^3, respectively). In addition, the partial loss of structural order must also be taken into account. Interestingly, the BET surface area and pore volume of mesoporous $LaFeO_3$ (83.2 m^2/g and 0.22 cm^3/g) are remarkably higher than those of the bulk $LaFeO_3$ (7.8 m^2/g and 0.04 cm^3/g).

A detailed study of the mesostructure $LaFeO_3$ is confirmed by the TEM images. In Fig. 3a, in addition to ordered mesoporous structure, there are partly non-ordered mesoporous materials, which can be attributed to the $LaFeO_3$ precursor incompletely filled into the template pores. The similar phenomenon can also be observed from the other perovskite oxides synthesized by the nanocasting method [43–46]. From the high resolution TEM image shown in Fig. 3b, the mesostructured network and well crystalline walls can be observed. The lattice fringes corresponding to the (1 2 1) plane of orthorhombic perovskite $LaFeO_3$ are clearly visible. In Fig. 3a (inset), selected area electron diffraction (SAED) analysis shows that the as-synthesized mesoporous $LaFeO_3$ is polycrystalline.

The residual Si of the mesoporous $LaFeO_3$ from the template SBA-15 should be considered. From the ICP-MS analysis, we know that about 5% of Si is still present in the sample due to the strong interaction of silica with rare earth elements.

3.2. Humidity sensing characteristics

The dependence of impedance on the relative humidity for the sensor using the mesoporous $LaFeO_3$ was measured at various frequencies, as shown in Fig. 4. It can be observed that the impedance at various relative humidity is strongly affected by the measuring frequencies, especially at low humidity range. It is worth noting that the impedance greatly decreases by more than five orders magnitude (1.7×10^6 to 4.5 kΩ) when the relative humidity varies from 11% to 98% at 10 Hz, showing the highest humidity response and the best linearity in the entire humidity range. Hence, 10 Hz is chosen as the optimum operating frequency. For comparison, the humidity response of the bulk $LaFeO_3$ sensor was also measured and shown in Fig. 5. It can be seen that the impedance of the sensor using bulk $LaFeO_3$ changes by about three orders of magnitude at the same condition. The response of mesoporous $LaFeO_3$ is also much higher than that of the $LaFeO_3$ sensor reported in the previous paper [35]. The superior response coupled with linearity in the wide range humidity of the mesoporous $LaFeO_3$ sensor indicates its excellent potential in the practical applications.

The humidity hysteresis characteristics of the sensors using mesoporous (solid symbol) and bulk (hollow symbol) $LaFeO_3$ were also detected at 10 Hz as shown in Fig. 5. The squares in the figure

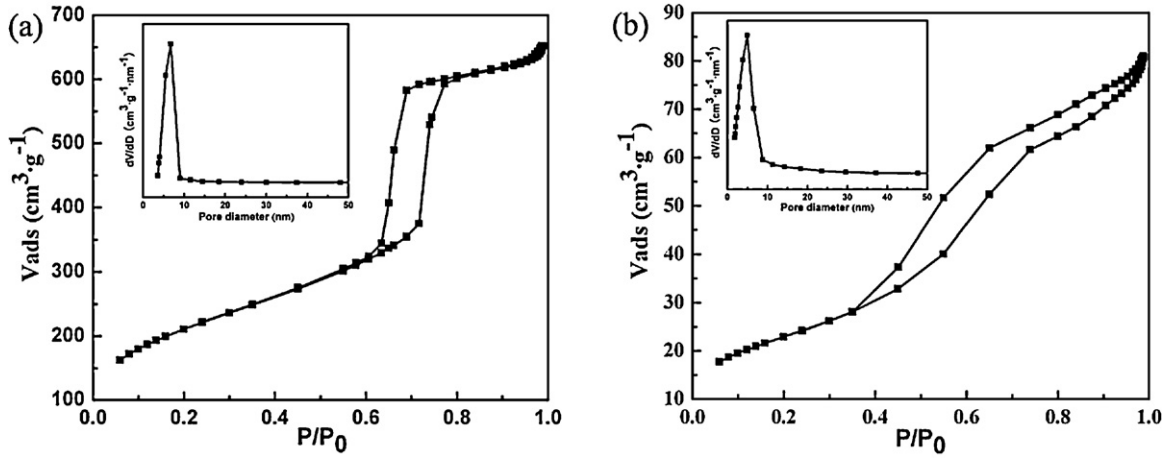

Fig. 2. Nitrogen adsorption–desorption isotherms and the corresponding pore size distribution of (a) SBA-15 and (b) mesoporous $LaFeO_3$.

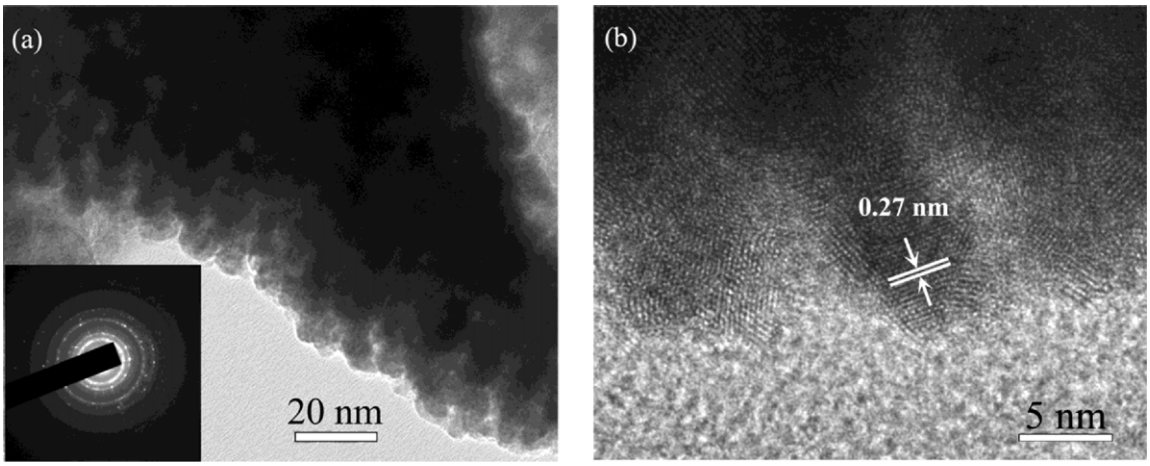

Fig. 3. (a) TEM image, SAED (inset) and (b) HRTEM image of mesoporous $LaFeO_3$.

stand for the course from low to high relative humidity, corresponding to the adsorption process. The dots express the opposite direction, corresponding to the desorption process. The hysteresis curves exhibit that the impedance in desorption process is lower than the adsorption, and the largest humidity hysteresis are about 4% and 16% for the sensors using the mesoporous and bulk $LaFeO_3$, respectively. Adsorption is an exothermic and spontaneous process while desorption is more difficult for the higher bonding energy between the adsorbed water molecules and the surface of sensing material [47,48]. Therefore, it leads to the hysteresis between the adsorption and desorption processes. The relative lower humidity hysteresis of the mesoporous $LaFeO_3$ sensor demonstrates its good performance as a humidity sensor. The response and recovery behavior, corresponding to water molecules adsorption and desorption process, is also important for humidity sensors. The response time is defined as the time taken by the sensor to reach 90% of the total impedance change when the sensor is switched from 11% to 98% RH, and the recovery time corresponding to the case of desorption (from 98% to 11% RH). The response and recovery characteristic curves of the sensors using the mesoporous and bulk $LaFeO_3$ are evaluated continuously at the frequency of 10 Hz and displayed in Fig. 6. The response times of the mesoporous and bulk $LaFeO_3$ sensors are both about 1 s, and the recovery time are about 148 s and 36 s, respectively. Both of them exhibit the excellent response performance. The relatively longer recovery times of the mesoporous $LaFeO_3$ sensor can be ascribed to the higher humidity sensitivity response and higher bonding energy between the adsorbed water molecules and the surface of the sensor material.

The long-term stability of the ceramic humidity sensor is also important for practical application. Herein, the stability of the mesoporous $LaFeO_3$ sensor was monitored under different humidity conditions for 6 months (Fig. 7). It can be observed that the impedance just varies slightly over the entire humidity region, indicating that the mesoporous $LaFeO_3$ sensor displays excellent long-term stability.

3.3. Humidity sensing mechanism

The conduction mechanism about the porous ceramic humidity sensors originates from chemical and physical adsorption of water molecules on their surface as well as the capillary condensation of water inside the pores [49,50]. Initially, at the low RH, the water

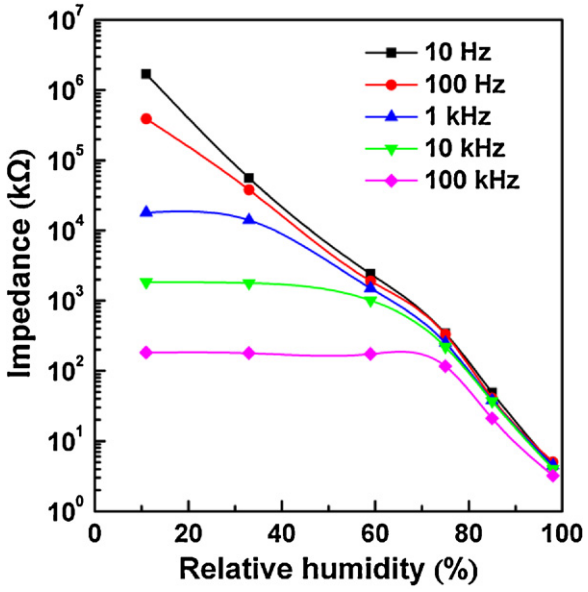

Fig. 4. The dependence of impedance on the relative humidity for the sensor based on the mesoporous $LaFeO_3$ measured at various frequencies.

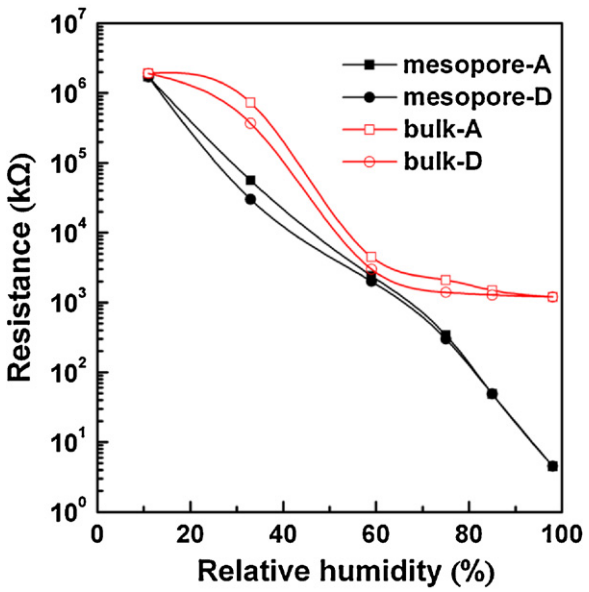

Fig. 5. The humidity hysteresis characteristic of the mesoporous $LaFeO_3$ sensor measured at 10 Hz.

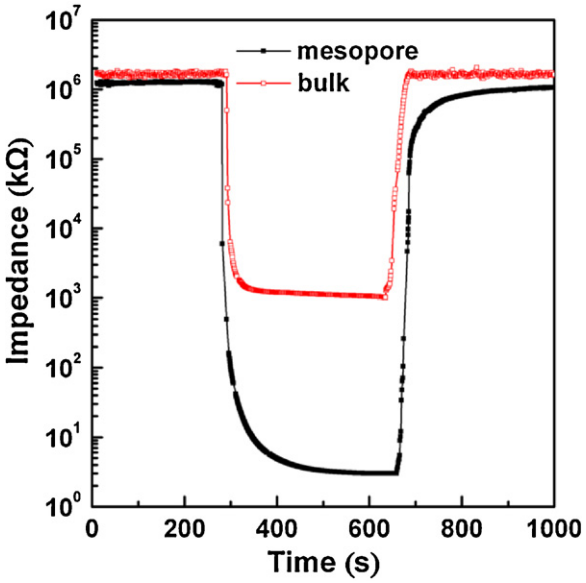

Fig. 6. The response and recovery characteristic curves of the mesoporous and bulk $LaFeO_3$ sensor measured at 10 Hz.

molecule is mainly chemisorbed onto the surface active sites of the sensing material [49,51]. A dissociating mechanism leads to the formation of a hydroxyl (OH^-) and a proton (H^+). The former is chemisorbed on the surface metal cations present in the surface layer of the grains and the latter associates with the surface O^{2-} group to form a second hydroxyl group. Protons originating from the dissociation hydroxyl groups as the charge carriers will hop between the hydroxyl groups [52]. It can be understood that the conduction process of the sensor mainly originates from the water adsorption on the sample surface. Therefore, the excellent properties of sensor based on the mesoporous $LaFeO_3$ are related to the higher surface area and porosity which provide more active sites for water adsorption, and finally offer more charge carriers for electrical conduction.

The chemisorbed layer, once formed, is not further affected by exposure to humidity. Subsequent water molecules are physically adsorbed on the hydroxyl layer by double hydrogen bonds with the oxygen atoms of the water molecule. In this stage, the surface coverage is not complete. Hydronium is the dominant charge carrier and H^+ migrate between the adjacent water molecules in clusters [53].

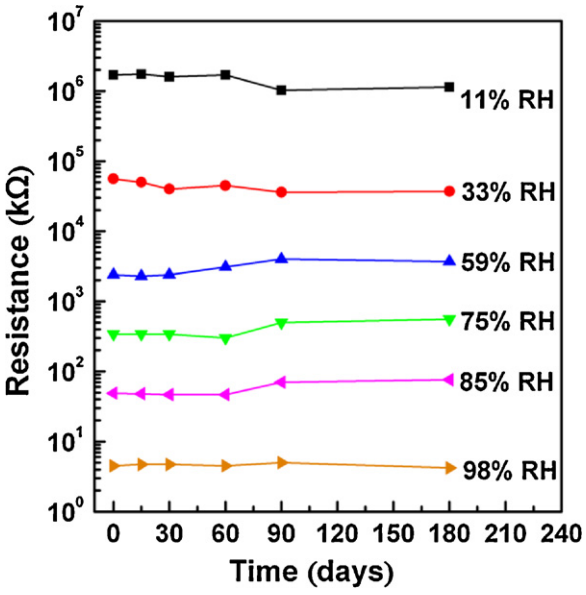

Fig. 7. The stability of the mesoporous $LaFeO_3$ sensor monitored at different humidity conditions for 6 months.

With the increase of the RH, when water molecules are abundant, the physisorbed water dissociates due to the high electrostatic field in the chemisorbed water: $2H_2O \rightarrow H_3O^+ + OH^-$ [13]. Water molecules become gradually identical to bulk liquid water, with H_3O^+ being hydrated and releasing a proton, $H_3O^+ \rightarrow H_2O + H^+$. The charge transport is governed by proton transfer between adjacent water molecules in the continuous water film. This process is known as the Grotthuss chain reaction [54].

With a further increasing of the humidity, the interaction between the porous structure and water must also be considered. The multilayers of physisorbed water molecules tend to condense in capillary pores with a radius below the Kelvin radius [6]. The effect is described by Kelvin equation [6,50]:

$$r_k = \frac{2\gamma M}{\rho RT \ \ln(P_s/P)} \quad (1)$$

where r_k is the Kelvin radius, γ is the surface tension, M is the molecular weight of water, ρ is the density of water, R is the gas constant, T is the absolute temperature, P_s and P are the water vapor pressure at saturation and the actual value, respectively.

Electrochemical impedance analysis is an effective method to study the various kinds of sensing properties [55,56]. To further explain the sensing mechanisms of the as-prepared mesoporous $LaFeO_3$ sensor, the measured and simulated complex impedance spectra (Nyquist plot) based on the mesoporous $LaFeO_3$ sensor were recorded in the frequency range from 0.5 Hz to 150 kHz, with the relative humidity varying from 11% to 98% at the room temperature, respectively (Fig. 8). It is obviously observed that the equivalent circuit model fits the measured data well. At low RH (11%), the complex impedance diagram shows a semicircle with a large radius of curvature. It is well known that semicircle represents a resistor R, in parallel with a capacitor C in the impedance spectra [57]. At moderate RH (33%, 59% and 75%), each curve are composed by a semicircle in the high frequency region and a straight line in the low frequency region. The straight line in the low frequency region represents Warburg behavior [58], which is related to the diffusion phenomena at the electrode–electrolyte interface and electrolytic conduction within the water condensed inside the mesopores of the sensing material. At high RH (85% and 95%), the semicircle become ignorable in the high frequency and only a straight line is observed at full frequency range. The equivalent circuit was modeled by Zview software and shown in Fig. 9a. The variation of R, C obtained by the simulated data for the mesoporous $LaFeO_3$ sensor as a function of RH is shown in Fig. 9b. The resistance is linear approximation, varying from 10^9 to 10^3 Ω with the RH increasing from 11% to 98%, which is rather similar with the change of the impedance in Fig. 4. The capacitance changed slightly in the entire humidity range. Thus, it is concluded that Zw is an important parameter to influence the complex impedance with the increase of RH, while the influence of the capacitance can be ignored.

Furthermore, the improvement of the humidity sensing performance for the mesoporous $LaFeO_3$ sensor results from the satisfying advantages correlated to the unique architecture of mesopores. The high surface area and pore volume which render the exposure of accessible active sites facilitate the adsorption and desorption of water molecules on the internal and external surface of the sensing material. The pore (about 4.9 nm) in the range of mesoporous structure will favor the ions diffusion, and therefore enhancing the high rate transport throughout the sensor.

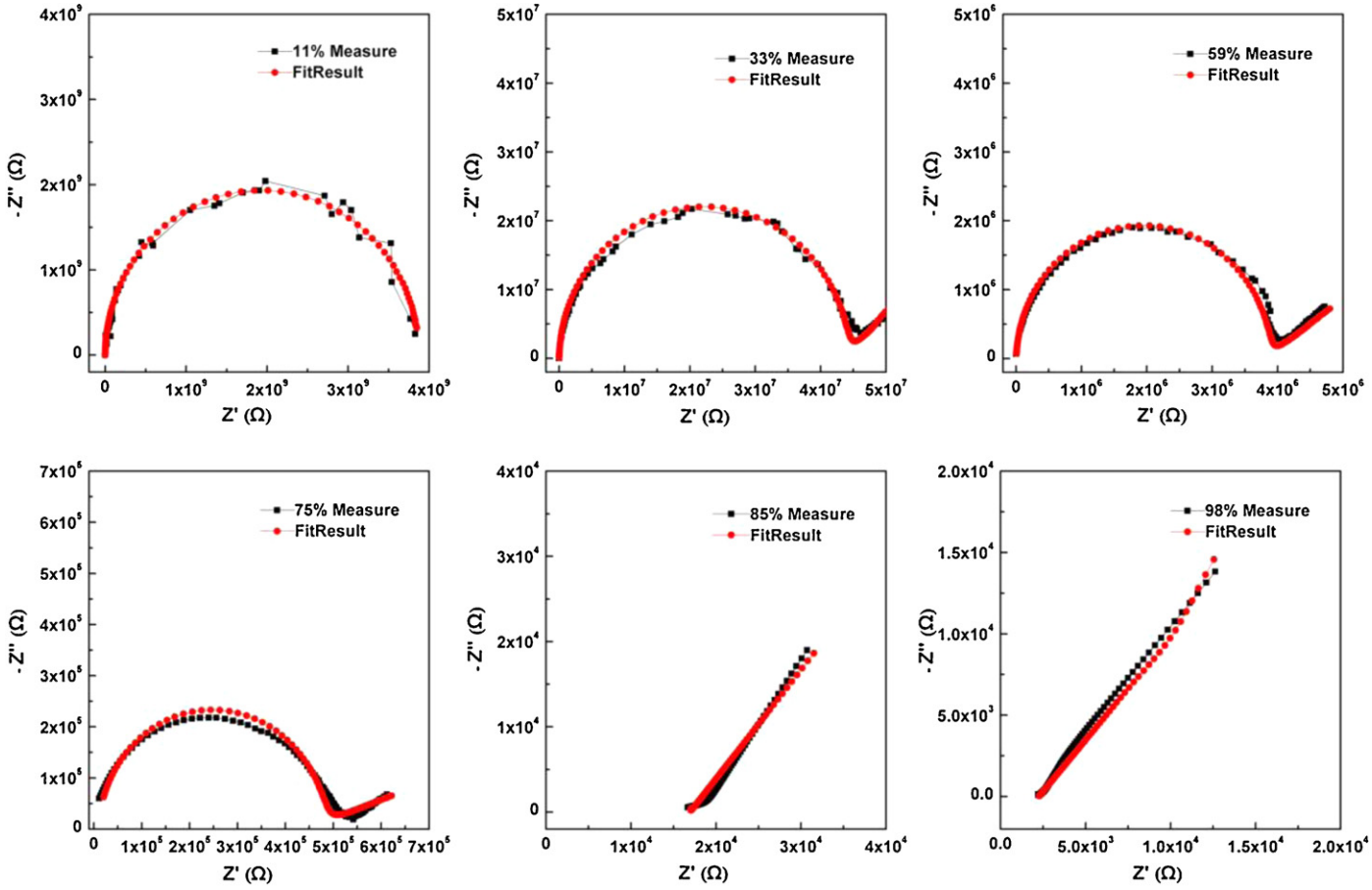

Fig. 8. The measured and simulated complex impedance spectra (Nyquist plot) based on mesoporous $LaFeO_3$ sensor with the frequency from 0.5 Hz to 150 kHz, RH varying from 11% to 98%.

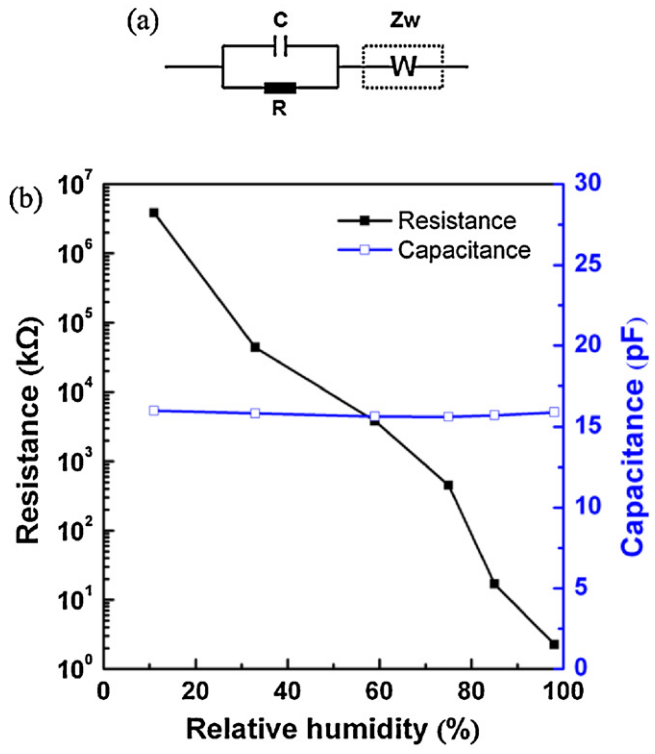

Fig. 9. (a) The equivalent circuit was modeled using Zview software and (b) the variation of *R*, *C* obtained by the simulated data based on mesoporous $LaFeO_3$ sensor with RH varying from 11% to 98%.

4. Conclusions

Mesoporous $LaFeO_3$ was successfully synthesized via the nanocasting method by using SBA-15 as a replica matrix. A ceramic humidity sensor based on the mesoporous $LaFeO_3$ was fabricated and evaluated. Humidity sensing measurements reveal that impedance greatly changes by more than five orders magnitude when the relative humidity varies from 11% to 98% at 10 Hz, and it also displays high response, fast response time, low hysteresis and long-time stability in the entire humidity region. The sensing mechanism of humidity sensors was interpreted by the complex impedance spectra (Nyquist plot). Furthermore, the sensor based on the mesoporous $LaFeO_3$ displays the higher response compared with that of bulk $LaFeO_3$ prepared by the sol–gel method. It can be concluded that thus-obtained mesoporous $LaFeO_3$ is an excellent material for application as humidity sensor because of their high surface area and pore volume with mesoporous structure.

Acknowledgements

This work was supported by Natural Science Foundation of China (Nos. 21001051, 61074172, 61134010), Program for Changjiang Scholars and Innovative Research Team in University (No. IRT1017) and Jilin Province Science and Technology Development Plan Program (20106002).

References

[1] U. Dellwo, P. Keller, J.-U. Meyer, Fabrication and analysis of a thick-film humidity sensor based on $MnWO_4$, Sensors and Actuators A 61 (1997) 298–302.

[2] N. Yamazoe, Y. Shimizu, Humidity sensors: principles and applications, Sensors and Actuators 10 (1986) 379–398.
[3] Z.M. Rittersma, A. Splinter, A. Bödecker, W. Benecke, A novel surface-micromachined capacitive porous silicon humidity sensor, Sensors and Actuators B 68 (2000) 210–217.
[4] K.S. Chou, T.K. Lee, F.J. Liu, Sensing mechanism of a porous ceramic as humidity sensor, Sensors and Actuators B 56 (1999) 106–111.
[5] T. Nltta, Ceramic humidity sensor, Industrial and Engineering Chemistry Product Research and Development 20 (1981) 669–674.
[6] E. Traversa, Ceramic sensors for humidity detection: the state-of-the-art and future developments, Sensors and Actuators B 23 (1995) 135–156.
[7] P.G. Su, C.C. Shiu, Electrical and sensing properties of a flexible humidity sensor made of polyamidoamine dendrimer–Au nanoparticles, Sensors and Actuators B 165 (2012) 151–156.
[8] M.M. Hawkeye, M.J. Brett, Optimized colorimetric photonic-crystal humidity sensor fabricated using glancing angle deposition, Advanced Functional Materials 21 (2011) 3652–3658.
[9] T.L. Yeo, T. Sun, K.T.V. Grattan, Fibre-optic sensor technologies for humidity and moisture measurement, Sensors and Actuators A 144 (2008) 280–295.
[10] P.R. Wiederhold, Water Vapor Measurement—Methods and Instrumentation, Marcel Dekker, New York, 1997.
[11] J.C. Tellis, C.A. Strulson, M.M. Myers, K.A. Kneas, Relative humidity sensors based on an environment-sensitive fluorophore in hydrogel films, Analytical Chemistry 83 (2011) 928–932.
[12] T. Morimoto, M. Nagao, F. Tokuda, The relation between the amounts of chemisorbed and physisorbed water on metal oxides, Journal of Physical Chemistry 73 (1969) 243–248.
[13] B.M. Kulwicki, Humidity sensors, Journal of the American Ceramic Society 74 (1991) 697–706.
[14] B. Cheng, B. Tian, C. Xie, Y. Xiao, S. Lei, Highly sensitive humidity sensor based on amorphous Al_2O_3 nanotubes, Journal of Materials Chemistry 21 (2011) 1907–1912.
[15] Y. Shimizu, H. Arai, T. Seiyama, Theoretical studies on the impedance–humidity characteristics of ceramic humidity sensors, Sensors and Actuators 7 (1985) 11–22.
[16] T.T. Emons, J.Q. Li, L.F. Nazar, Synthesis and characterization of mesoporous indium tin oxide possessing an electronically conductive framework, Journal of the American Chemical Society 124 (2002) 8516–8517.
[17] J. Liu, S.Z. Qiao, Q.H. Hu, G.Q. Lu, Magnetic nanocomposites with mesoporous structures: synthesis and applications, Small 7 (2011) 425–443.
[18] A. Rumplecker, F. Kleitz, E. Salabas, F. Schüth, Hard templating pathways for the synthesis of nanostructured porous Co_3O_4, Chemistry of Materials 19 (2007) 485–496.
[19] Y. Ren, Z. Ma, P.G. Bruce, Ordered mesoporous metal oxides: synthesis and applications, Chemical Society Reviews 41 (2012) 4909–4927.
[20] B. Tian, X. Liu, H. Yang, S. Xie, C. Yu, B. Tu, D. Zhao, General synthesis of ordered crystallized metal oxide nanoarrays replicated by microwave-digested mesoporous silica, Advanced Materials 15 (2003) 1370–1374.
[21] S.C. Laha, R. Ryoo, Synthesis of thermally stable mesoporous cerium oxide with nanocrystalline frameworks using mesoporous silica templates, Chemical Communications 213 (2003) 2138–2139.
[22] H. Tüysüz, E.L. Salabas, E. Bill, H. Bongard, B. Spliethoff, C.W. Lehmann, F. Schüth, Synthesis of hard magnetic ordered mesoporous Co_3O_4/$CoFe_2O_4$ nanocomposites, Chemistry of Materials 24 (2012) 2493–2500.
[23] K.E. Shopsowitz, A. Stahl, W.Y. Hamad, M.J. MacLachlan, Hard templating of nanocrystalline titanium dioxide with chiral nematic ordering, Angewandte Chemie International Edition 51 (2012) 6886–6890.
[24] J. Roggenbuck, M. Tiemann, Ordered mesoporous magnesium oxide with high thermal stability synthesized by exotemplating using CMK-3 carbon, Journal of the American Chemical Society 127 (2005) 1096–1097.
[25] X. Lai, X. Li, W. Geng, J. Tu, J. Li, S. Qiu, Ordered mesoporous copper oxide with crystalline walls, Angewandte Chemie International Edition 46 (2007) 738–741.
[26] W. Yue, W. Zhou, Crystalline mesoporous metal oxide, Progress in Natural Science 18 (2008) 1329–1338.
[27] E. Ramasamy, J. Lee, Ordered mesoporous Zn-doped SnO_2 synthesized by exotemplating for efficient dye-sensitized solar cells, Energy & Environmental Science 4 (2011) 2529–2536.
[28] T. Wagner, C-D. Kohl, S. Morandi, C. Malagù, N. Donato, M. Latino, G. Neri, M. Tiemann, Photoreduction of mesoporous In_2O_3: mechanistic model and utility in gas sensing, Chemistry-A European Journal 18 (2012) 8216–8223.
[29] E. Rossinyol, A. Prim, E. Pellicer, J. Arbiol, F. Hernández-Ramírez, F. Peiró, A. Cornet, J.R. Morante, L.A. Solovyov, B. Tian, T. Bo, D. Zhao, Synthesis and characterization of chromium-doped mesoporous tungsten oxide for gas-sensing applications, Advanced Functional Materials 17 (2007) 1801–1806.
[30] Y. Wang, J. Ren, Y. Wang, F. Zhang, X. Liu, Y. Guo, G. Lu, Nanocasted synthesis of mesoporous $LaCoO_3$ perovskite with extremely high surface area and excellent activity in methane combustion, Journal of Physical Chemistry C 112 (2008) 15293–15298.
[31] J.W. Fergus, Perovskite oxides for semiconductor-based gas sensors, Sensors and Actuators B 123 (2007) 1169–1179.
[32] R.J.H. Voorhoeve, D.W. Johnson Jr., J.P. Remeika, P.K. Gallagher, Perovskite oxides: materials science in catalysis, Science 195 (1977) 827–833.
[33] R.E. Cohen, Origin of ferroelectricity in perovskite oxides, Nature 358 (1992) 136–138.
[34] E.J. Crumlin, S.J. Ahh, D. Lee, E. Mutoro, M.D. Biegalski, H.M. Christen, S.H. Yang, Oxygen electrocatalysis on epitaxial $La_{0.6}Sr_{0.4}CoO_3$-delta perovskite thin films for solid oxide fuel cells, Journal of the Electrochemical Society 159 (2012) 219–225.
[35] J. Wang, F.Q. Wu, K.H. Shi, X.H. Wang, P.P. Sun, Humidity sensitivity of composite material of lanthanum ferrite/polymer quaternary acrylic resin, Sensors and Actuators B 99 (2004) 586–591.
[36] S. Zhao, J.K.O. Sin, B. Xu, M. Zhao, Z. Peng, H. Cai, A high performance ethanol sensor based on field-effect transistor using a $LaFeO_3$ nano-crystalline thin-film as a gate electrode, Sensors and Actuators B 64 (2000) 83–87.
[37] N.N. Toan, S. Saukko, V. Lantto, Gas sensing with semiconducting perovskite oxide $LaFeO_3$, Physica B 327 (2003) 279–282.
[38] H. Aono, E. Traversa, M. Sakamoto, Y. Sadaoka, Crystallographic characterization and NO_2 gas sensing property of $LnFeO_3$ prepared by thermal decomposition of Ln–Fe hexacyanocomplexes, $Ln[Fe(CN)_6]\cdot nH_2O$, Ln = La, Nd, Sm, Gd, and Dy, Sensors and Actuators B 94 (2003) 132–139.
[39] I. Rivas, J. Alvarez, E. Pietri, M.J. Pérez-Zurita, M.R. Goldwasser, Perovskite-type oxides in methane dry reforming: effect of their incorporation into a mesoporous SBA-15 silica-host, Catalysis Today 149 (2010) 388–393.
[40] P. Song, Q. Wang, Z. Zhang, Z. Yang, Synthesis and gas sensing properties of biomorphic $LaFeO_3$ hollow fibers templated from cotton, Sensors and Actuators B 147 (2010) 248–254.
[41] D. Zhao, Q. Huo, J. Feng, B.F. Chmelka, G.D. Stucky, Nonionic triblock and star diblock copolymer and oligomeric surfactant syntheses of highly ordered, hydrothermally stable, mesoporous silica structures, Journal of the American Chemical Society 120 (1998) 6024–6036.
[42] C. Vázquez-Vázquez, P. Kógerler, M.A. López-Quintela, Preparation of $LaFeO_3$ particles by sol–gel technology, Journal of Materials Research 13 (1998) 451–456.
[43] R.K.C. de Lima, M.S. Batista, M. Wallau, E.A. Sanches, Y.P. Mascarenhas, E.A. Urquieta-González, High specific surface area LaFeCo perovskites—synthesis by nanocasting and catalytic behavior in the reduction of NO with CO, Applied Catalysis B: Environmental 90 (2009) 441–450.
[44] H. Su, L. Jing, K. Shi, C. Yao, H. Fu, Synthesis of large surface area $LaFeO_3$ nanoparticles by SBA-16 template method as high active visible photocatalysts, Journal of Nanoparticle Research 12 (2010) 967–974.
[45] S.V. Nguyen, V. Szabo, D. Trong On, S. Kaliaguine, Mesoporous silica supported $LaCoO_3$ perovskites as catalysts for methane oxidation, Microporous and Mesoporous Materials 54 (2002) 51–61.
[46] J. Deng, L. Zhang, H. Dai, C.T. Au, In situ hydrothermally synthesized mesoporous $LaCoO_3$/SBA-15 catalysts: high activity for the complete oxidation of toluene and ethyl acetate, Applied Catalysis A-General 352 (2009) 43–49.
[47] W. Qu, W. Wlodarski, J. Meyer, Comparative study on micromorphology and humidity sensitive properties of thin-film and thick-film humidity sensors based on semiconducting $MnWO_4$, Sensors and Actuators B 64 (2000) 76–82.
[48] K. Ocakoglu, S. Okur, Humidity sensing properties of novel ruthenium polypyridyl complex, Sensors and Actuators B 151 (2010) 223–228.
[49] P.M. Faia, C.S. Furtado, A.J. Ferreira, Humidity sensing properties of a thick-film titania prepared by a slow spinning process, Sensors and Actuators B 101 (2004) 183–190.
[50] P.M. Faia, C.S. Furtado, A.J. Ferreira, AC impedance spectroscopy: a new equivalent circuit for titania thick film humidity sensors, Sensors and Actuators B 107 (2005) 353–359.
[51] Z. Chen, C. Lu, Humidity sensors: a review of materials and mechanisms, Sensor Letters 3 (2005) 274–295.
[52] J.H. Anderson, G.A. Parks, The electrical conductivity of silica gel in the presence of adsorbed water, Journal of Physical Chemistry 72 (1968) 3662–3668.
[53] Y.C. Yeh, T.Y. Tseng, D.A. Chang, Electrical properties of TiO_2–$K_2Ti_6O_{13}$ porous ceramic humidity sensor, Journal of the American Ceramic Society 73 (1990) 1992–1998.
[54] F.M. Ernsberger, The nonconformist ion, Journal of the American Ceramic Society 66 (1983) 747–750.
[55] J.E. Bauerle, Study of solid electrolyte polarization by a complex admittance method, Journal of Physics and Chemistry of Solids 30 (1969) 2657–2670.
[56] H. Gu, X. Su, K.P. Loh, Electrochemical impedance sensing of DNA hybridization on conducting polymer film-modified diamond, Journal of Physical Chemistry B 109 (2005) 13611–13618.
[57] G. Gusmano, G. Montesperelli, E. Traversa, Microstructure and electrical properties of $MgAl_2O_4$ thin films for humidity sensing, Journal of the American Ceramic Society 76 (1993) 743–750.
[58] P. Christensen, A. Hammett, Techniques and Mechanisms in Electrochemistry, Springer, Netherlands, 1994.

Biographies

Jing Zhao received her MS degree in chemistry, Jilin University, China in 2010. She entered the PhD course in 2010, majored in microelectronics and solid-state electronics. Now, she is engaged in the synthesis and characterization of the functional materials and chemical sensors.

Yinping Liu received her BS degree from the electronics information and engineering department, Jilin University, China in 2011. Presently, she is a graduate student, majored in integrated circuit Engineering.

Xiaowei Li received his BS degree from the electronics information and engineering department, Jilin University, China in 2011. Presently, he is a graduate student, majored in integrated circuit engineering.

Geyu Lu received his BS and MS degree in electronic sciences from Jilin University, China in 1985 and 1988, respectively, and PhD degree in 1998 from Kyushu University in Japan. Now he is a professor of Jilin University, China. Presently, he is interested in the development of functional materials and chemical sensors.

Lu You received his BS degree from the electronics science and engineering department, Jilin University, China in 2010. Presently, he is a graduate student, majored in microelectronics and solid state electronics.

Xishuang Liang received the BEng degree in department of electronic science and technology in 2004. He received his Doctor's degree in College of Electronic Science and Engineering at Jilin University in 2009. Now he is a lecturer of Jilin University, China. His current research is solid electrolyte gas sensor.

Fengmin Liu received the BE degree in department of electronic science and technology in 2000. She received her Doctor's degree in College of Electronic Science and Engineering at Jilin University in 2005. Now she is an associate professor in Jilin University, China. Her current research is preparation and application of semiconductor oxide, especial in gas sensor and solar cell.

Tong Zhang received her MS degree in major of semiconductor materials in 1992, and PhD degree in the field of microelectronics and solid-state electronics in 2001 from Jilin University. She was appointed a full professor in College of Electronics Science and Engineering, Jilin University in 2001. Now, she is interested in the field of sensing functional materials and gas sensors and humidity sensors.

Yu Du received her PhD from chemistry of Jilin University, China in 2006. After that, she had been working as the postdoctoral at Nanyang Technological University, Singapore for about two years. She is currently an associate professor at the electronics science and engineering department of Jilin University, China. Her current research interests are nanoscience and gas sensors.